Liquid Crystals
Publication details, including instructions for authors and subscription information:
http://www.informaworld.com/smpp/title~content=t713926090

Degeneracy lifting near the frustration points due to long-range interlayer interaction forces and the resulting varieties of polar chiral tilted smectic phases

K. L. Sandhya[a]; J. K. Vij[a]; Atsuo Fukuda[a]; A. V. Emelyanenko[b]
[a] Department of Electronic and Electrical Engineering, Trinity College, University of Dublin, Ireland [b] Department of Physics, Moscow State University, Moscow, Russia

First published on: 26 August 2009

To cite this Article Sandhya, K. L. , Vij, J. K. , Fukuda, Atsuo and Emelyanenko, A. V.(2009) 'Degeneracy lifting near the frustration points due to long-range interlayer interaction forces and the resulting varieties of polar chiral tilted smectic phases', Liquid Crystals, 36: 10, 1101 — 1118, First published on: 26 August 2009 (iFirst)
To link to this Article: DOI: 10.1080/02678290902815434
URL: http://dx.doi.org/10.1080/02678290902815434

Liquid Crystals,
Vol. 36, Nos. 10–11, October–November 2009, 1101–1118

Taylor & Francis
Taylor & Francis Group

INVITED ARTICLE

Degeneracy lifting near the frustration points due to long-range interlayer interaction forces and the resulting varieties of polar chiral tilted smectic phases

K.L. Sandhya[a], J.K. Vij[a], Atsuo Fukuda[a]* and A.V. Emelyanenko[b]

[a]*Department of Electronic and Electrical Engineering, Trinity College, University of Dublin, Dublin 2, Ireland;* [b]*Department of Physics, Moscow State University, Moscow 119992, Russia*

(Received 30 January 2009; final form 12 February 2009)

To gain a clear understanding of ferroelectricity and antiferroelectricity together with their frustration in chiral tilted smectic liquid crystals, we have constructed E–T phase diagrams by drawing field-induced birefringence contours in the prototype binary mixture system of MHPOCBC and MHPOOCBC. The results obtained are discussed in terms of the theoretical model proposed by Emelyanenko and Osipov; we have insisted on the appropriateness of specifying the biaxial subphases, which emerge sequentially in the temperature-induced transition, by the relative ratio of ferroelectric and antiferroelectric orderings in the superstructure unit cell, such as $\mathrm{Sm}C^*_A(q_T)$, where $q_T = [F]/([A] + [F])$. Additional subphases other than the ordinary subphases with three- and four-layer superstructures, $\mathrm{Sm}C^*_A(1/3)$ and $\mathrm{Sm}C^*_A(1/2)$, have been established to exist, firmly for $\mathrm{Sm}C^*_A(0 < q_T < 1/3)$ and less adequately for $\mathrm{Sm}C^*_A(1/3 < q_T < 1/2)$ and $\mathrm{Sm}C^*_A(1/2 < q_T < 1)$. Likewise, we have observed several stable superstructures during the field-induced transition from the biaxial subphases to unwound SmC*, and have tried to specify them using $q_E = |[R] - [L]|/([R] + [L])$, where $[R]$ and $[L]$ refer to the numbers of smectic layers with directors tilted to the right and to the left, respectively, in a unit cell of the superstructure. We have also found the characteristic field-induced deformation of the uniaxial subphase $\mathrm{Sm}C^*_\alpha$ and attempted to understand it in terms of the devil's staircase due to soliton condensation reported recently by Torikai and Yamashita (*41*).

Keywords: chiral tilted smectics; ferroelectricity; antiferroelectricity; frustration; subphase

1. Introduction

Chiral tilted smectic liquid crystals are the only fluids known to exhibit clear ferroelectricity and antiferroelectricity. The most common tilted smectic liquid crystal is the synclinic smectic C phase (SmC), where the in-layer director is tilted in the same direction and sense by an angle varying from 0 to 45°, the magnitude of which is dependent on both the material and temperature. On the other hand, the anticlinic smectic C_A phase ($\mathrm{Sm}C_\mathrm{A}$) with the tilt sense alternating from layer to layer has been observed in more restricted smectic materials. These chiral versions designated as SmC* and $\mathrm{Sm}C^*_A$ may become ferroelectric and antiferroelectric, respectively; the in-layer director shows a macroscopic helical structure with a pitch of the order of 1 μm and each smectic layer possesses a spontaneous polarisation, up to a few millcoulombs per square metre, nearly proportional to the tilt angle and perpendicular to the tilt plane with a sign determined by the tilting sense (*1*, *2*). All of the intermolecular interactions between smectic layers must be relatively weak, and this enables us to explain why a moderate applied electric field can switch from $\mathrm{Sm}C^*_A$ to SmC*. The switching accompanies the optical axis rotation from the smectic layer normal to the director tilt direction in an unwound SmC* state. The phase transition between $\mathrm{Sm}C^*_A$ and SmC* is of first order and the system is frustrated between the synclinic ferroelectric and anticlinic antiferroelectric orderings. The frustration in the non-tilted SmA phase is described in de Gennes's textbook (*3*), which shows that there appear several interesting frustrated phases. Likewise, the frustration causes the temperature-induced sequence of phase transitions and produces a variety of optically biaxial polar subphases between the main phases, $\mathrm{Sm}C^*_A$ and SmC* (see (*3–5*)).

There exist at least two biaxial subphases with superstructures consisting of three- and four-layer unit cells (*6*). Both subphase superstructures are not planar although quite biaxial, and are rather close to the Ising model but very different from the uniaxial clock model (*7–13*). Among several theoretical models (*14–27*), which differ mainly in the nature and origin of the long-range interlayer interaction, the one proposed by Emelyanenko and Osipov is most intuitively understandable from an experimental point of view. They showed that a simple discrete model can be used to describe the entire sequence of biaxial subphases and to determine the non-planar

*Corresponding author. Email: fukudaa@tcd.ie

ISSN 0267-8292 print/ISSN 1366-5855 online

DOI: 10.1080/02678290902815434
http://www.informaworld.com

structure of each subphase (*14–18*). They numerically calculated the subphase superstructures for unit cells consisting of up to nine smectic layers. The subphases emerging sequentially with increasing temperature have the superstructures with unit cells of nine, seven, five, eight, three and four smectic layers. When use is made of

$$q_T = \frac{[F]}{[A]+[F]}, \tag{1}$$

the emerging order now becomes monotonic, 1/9, 1/7, 1/5, 1/4, 1/3 and 1/2. Here $[A]$ and $[F]$ refer to the numbers of antiferroelectric and ferroelectric orderings in a unit cell. It appears reasonable to specify the biaxial subphases by their q_T even in the Emelyanenko–Osipov model, which is more realistic than the Ising model originally used in defining q_T; hereafter we designate them as $\mathrm{Sm}C_A^*(q_T)$ as in (*6*) and (*28*).

Now let us emphasise the important role of q_T from a general point of view. At sufficiently low temperatures, $\mathrm{Sm}C_A^*$ is stable and the anticlinic antiferroelectric orderings prevail throughout the smectic layer. Increasing the temperature may happen to excite some synclinic orderings and produce large-scale superstructures specified with increasing q_T. If the short-range interlayer interaction forces between adjacent layers alone are operative, however, none of them thus produced has a smaller free energy than that of $\mathrm{Sm}C_A^*$ or Sm*C**; the temperature-induced phase transition occurs directly between $\mathrm{Sm}C_A^*$ and Sm*C**. Any long-range interlayer interaction forces may stabilise some of these superstructures to exist as subphases in the finite temperature ranges. Since these forces are generally weak, the lower-temperature subphase is expected to have a smaller q_T than the higher-temperature subphase. This is the reason why the emerging order of the subphases with increasing temperature can be specified by monotonically increasing q_T. What is meaningful in specifying the emerging order is not the number of layers but the relative amount of ferroelectric and antiferroelectric orderings in the unit cell (*6*), i.e. the q_T number. In solid state physics, we frequently encounter such large-scale superstructures as those with periodicities of three and four layers. The presence of some form of frustration is common to their emergence; the frustration may allow us to disclose delicate effects, which otherwise are hard to detect.

Near the transition temperature to Sm*A*, the frustration may occur among the three main phases, $\mathrm{Sm}C_A^*$, Sm*C** and Sm*A*. The optically uniaxial polar $\mathrm{Sm}C_\alpha^*$ subphase may also emerge directly below Sm*A* and replace Sm*C** in some cases. This is an interesting subphase characterised by a *microscopic* short-pitch helical structure with several nanometres to several tens of nanometres pitches (*7*, *8*, *29–39*). Here the short pitch p_α is usually measured as the number of smectic layers in one turn, although not commensurate with the smectic layer, and continuously changes with temperature, monotonically increasing in some materials while decreasing in others. Cepic and Zeks were the first to predict the $\mathrm{Sm}C_\alpha^*$ short-pitch helical structure (*40*). Quite recently, Yamashita's group at Mie University theoretically studied the electric-field-induced phase transition from $\mathrm{Sm}C_\alpha^*$ to Sm*C* (unwound Sm*C**), i.e. the unwinding process of $\mathrm{Sm}C_\alpha^*$, as a condensation process of discrete solitons (*41–45*). This phase transition is a typical example of the nucleation type in contrast with the instability type (*46*). They found that the process exhibits a devil's staircase, and opened the way to understand the staircase character observed in the early stage of investigations on the $\mathrm{Sm}C_\alpha^*$ switching response to an applied electric field (*6, 47–49*).

Understanding clearly the ferroelectricity and antiferroelectricity together with their frustration in tilted smectic liquid crystals has become increasingly a matter of importance. In particular, it is still a major issue, in the disordered system such as smectics lacking truly long-range positional order, as to what long-range interlayer interaction forces can produce the biaxial subphase superstructures and the uniaxial $\mathrm{Sm}C_\alpha^*$ short pitch helical structure. The $\mathrm{Sm}C_A^*(1/3)$ subphase is of fundamental importance because it is a rare but typical example of the *ferrielectric* phase observed not only in liquid crystals but also in condensed materials in general (*6*, *10*, *50*, *51*); interestingly, it has the intrinsic instability which makes it difficult to determine the accurate structure (*22*, *52*). Such tilted smectics with characteristic polar properties are typically responsive nonlinearly to applied electric fields. In fact, our preliminary experimental study indicated that the field-induced nonlinear deformation of $\mathrm{Sm}C_\alpha^*$ is quite intriguing as reported in (*53*). The aim of this paper is to investigate the emerging sequence of various uniaxial and biaxial subphases, in particular, the biaxial phases other than the well-known $\mathrm{Sm}C_A^*(1/3)$ and $\mathrm{Sm}C_A^*(1/2)$, and to clarify their electric-field-induced deformation and resulting stable states in tilted smectic phases. For this purpose, we construct the *E–T* phase diagrams by drawing the field-induced birefringence contours in the prototype binary mixture system of MHPOCBC and MHPOOCBC. It is shown that the observed results can be well explained by the extended Emelyanenko–Osipov model (*14–18*) together with the condensation of discrete solitons recently proposed by Yamashita's group of Mie University (*41–46*).

2. Experiment

Samples used are the binary mixtures of MHPOCBC and MHPOOCBC, the chemical structures of which are given in Figure 1. The structures are quite similar and the only

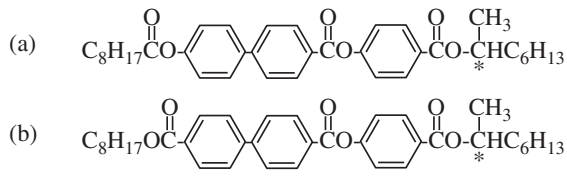

Figure 1. Chemical structures of samples used in the present experiments, both of which were the (*S*) moieties. The structures are quite similar and the only difference is in the achiral chain: (a) alkylcarboxy– in MHPOCBC; (b) alkoxycarbonyl– in MHPOOCBC.

difference is in the achiral chain: alkylcarboxy– in MHPOCBC while alkoxycarbonyl– in MHPOOCBC. The (*S*) moieties of both compounds were used in the present experiments. In the early stage of investigations on the subphases, the binary mixtures were systematically studied and the *E–T* phase diagrams were obtained by observing conoscopic figures in homeotropically aligned cells (*28*). In previous papers (*16*, *54*, *55*) it was shown that drawing birefringence contours in the *E–T* phase diagram is much easier and more informative than observing conoscopic figures. The contours showed such characteristic patterns that the typical uniaxial and biaxial subphases SmC^*_α, Sm$C^*_A(1/2)$ and Sm$C^*_A(1/3)$, as well as the fundamental phases Sm*A*, Sm*C** and SmC^*_A, can easily be identified. Although complementary measurements are possible in homogeneously aligned cells as actually performed by Orihara *et al.* (*56*), homeotropically aligned cells are mostly free from the interface effects and are informative and useful in studying the subphases particularly in the low field regions. To check the existence of subphases other than Sm$C^*_A(1/3)$ and Sm$C^*_A(1/2)$, we also measured the Bragg reflection spectra by using a ultraviolet (UV)/visible–infrared (IR) spectrophotometer (Perkin-Elmer, Lambda 900).

The field-induced birefringence was actually measured by using a photo-elastic modulator (PEM), which is also designated as a piezo-optical modulator (POM) or a stress plate modulator (SPM). It was first constructed in 1966 by Billardon and Badoz and since then several modifications have been reported by many investigators (*57–62*). A PEM is a waveplate, whose retardation varies sinusoidally with time depending on the applied AC voltage. Preparing a self-made PEM was not a difficult task, but here we chose a more convenient method: we used a commercial one, PEM-90 (Hinds Instruments, Hillsboro, OR) with a resonant frequency of 50 kHz. The PEM modulation method with a lock-in amplifier is much superior to the traditional static method with a compensator. Detailed explanations were given in previous papers (*16*, *55*) for the PEM-based setup of measuring field-induced birefringence and for the method to determine the retardation,

$$\Delta = (2\pi d/\lambda)|\Delta n| = \Delta' + m\pi, \qquad (2)$$

without using a standard quarter-wave or half-wave plate, where $0 \leq \Delta' \leq 2\pi$, $m = 0,1,2,\ldots$, and d, λ and Δn are the cell thickness, He–Ne laser wavelength and field-induced birefringence, respectively.

There exists a vague idea that the phase boundaries in the *E–T* phase diagram must be sharp lines. Actually, however, some of them may not be so sharp but rather broad in the *E–T* phase diagram with birefringence contour lines so far obtained in homeotropic cells (*16*, *54*, *55*). One of the reasons for the broad boundaries results from the temperature resolution of 0.1°C used in the actual measurements; the field-induced birefringence was measured at a particular temperature by changing the applied field stepwise at an interval of 8.33 mV μm^{-1} and the temperature was lowered also stepwise at an interval of 0.1°C. The temperature resolution becomes conspicuous when use is made of the expanded temperature axis to show clearly the existence of some subphases in narrow temperature ranges. In addition to this experimental restriction, several rather intrinsic causes are conceivable for the broad boundaries.

(1) The first-order transition occurs inhomogeneously through the solitary wave propagation as studied in detail for SmC^*_A–SmC^*, the propagation speed of which becomes zero at the critical field as well as at the critical temperature.
(2) Large deformation can easily occur even in a single phase and results in a change of birefringence sensitively.
(3) Some subphases may become unstable under an applied field.
(4) Even at zero field some others may be intrinsically unstable as Sm$C^*_A(1/3)$.

3. Results and discussion

3.1 Global evolution of subphase emerging sequence

3.1.1 Experimental evidence for the emergence of biaxial subphases other than *Sm*$C^*_A(1/3)$ and *Sm*$C^*_A(1/2)$

We have obtained the *E–T* phase diagrams for MHPOCBC binary mixtures containing MHPOOCBC with 0, 12, 25, 38, 50, 55, 60, 65, 70, 85, 89 and 93 wt% in homeotropic cells using the procedure described in reference 16. The *E–T* phase diagrams for these mixtures are summarised in Figure 2. In pure MHPOCBC, the phase emerging sequence is rather simple, SmC^*_A – SmC^*_α – Sm*A*. Between 25 and 38 wt%, Sm$C^*_A(1/3)$ is stabilised; Sm$C^*_A(1/2)$ emerges between

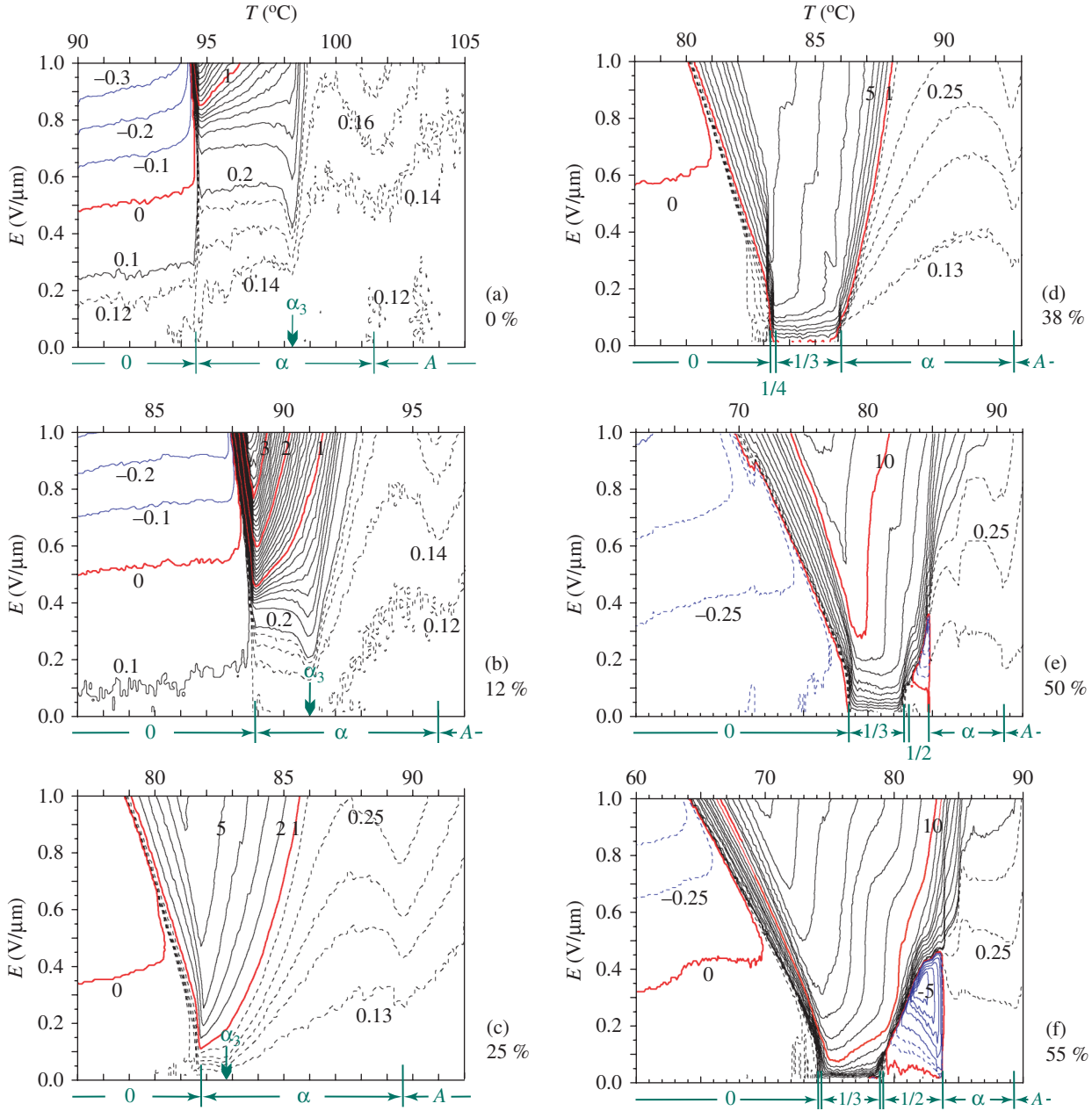

Figure 2. *E–T* phase diagrams for MHPOCBC binary mixtures containing MHPOOCBC with several concentrations. The temperature range of each phase at $E = 0$ is shown in the lower part, where α and A indicate SmC^*_α and SmA, respectively, and the numbers refer to q_T; note that SmC^*_A and SmC* have $q_T = 0$ and 1, respectively. An arrow with α_3 in (a), (b) and (c) shows the temperature where the microscopic short-pitch of SmC^*_α is considered to become $p_\alpha = 3$ smectic layers. Birefringence contours are drawn by solid lines at an interval of $\Delta n = 0.1 \times 10^{-3}$ in (a) and (b) or 1×10^{-3} in others; some auxiliary contours are given by dotted lines appropriately for convenience. Contour lines may form negative closed loops in the antiferroelectric SmC^*_A and Sm$C^*_A(1/2)$ temperature ranges. The field-induced stable states specified by q_E given in Equation (5) appear as the vertical parts of contour lines. As seen in the contour lines of $\Delta n = 7 \times 10^{-3}$ in (d) and of $\Delta n = 19 \times 10^{-3}$ in (i), some of the stable states emerge stepwise, indicating the staircase character of the field-induced stable states. These may correspond to $q_E = 1/3$, 1/2 and 3/5 states. Furthermore, the staircase character of the field-induced unwinding process of SmC^*_α microscopic short pitch helical structure is also clearly seen in (e) and (f). See the text for details.

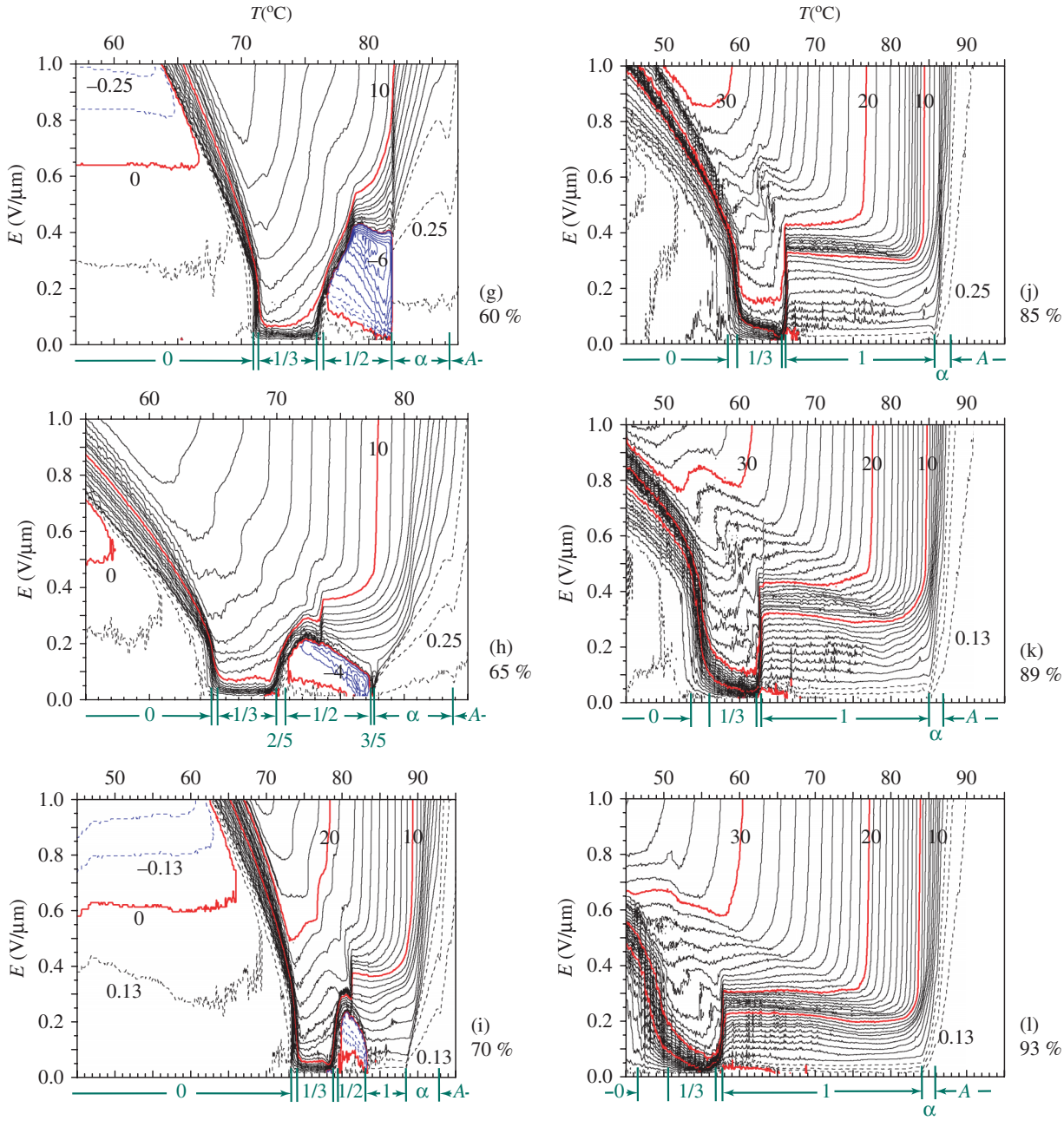

Figure 2. (*Continued*)

38 and 50 wt%, but disappears between 70 and 85 wt% again. Before the disappearance of Sm$C_A^*(1/2)$, SmC^* emerges between 65 and 70 wt%. In pure MHPOOCBC, it looks like Sm$C_A^*(1/3)$ does not appear before crystallisation. Thus, the global evolution of phase emerging sequence is:

(1) SmC_A^*–SmC_α^*–SmA;
(2) SmC_A^*–Sm$C_A^*(1/3)$–SmC_α^*–SmA;
(3) SmC_A^*–Sm$C_A^*(1/3)$–Sm$C_A^*(1/2)$–SmC_α^*–SmA;
(4) SmC_A^*–Sm$C_A^*(1/3)$–Sm$C_A^*(1/2)$–SmC^*–SmC_α^*–SmA;
(5) SmC_A^*–Sm$C_A^*(1/3)$–SmC^*–SmC_α^*–SmA;
(6) SmC_A^*–SmC^*–SmC_α^*–SmA.

Such an evolution of (1)–(6) has been observed in various systems of binary mixture including racemisation. Moreover, in lots of single compounds and mixtures, one of the above phase sequences has been found. A common origin must underlie the mechanism

responsible for the emergence of the three subphases, biaxial Sm$C_A^*(1/3)$ and Sm$C_A^*(1/2)$ together with uniaxial SmC_α^*, as widely accepted in the liquid crystal community.

What we would like to emphasise here is the emergence of biaxial subphases other than Sm$C_A^*(1/3)$ and Sm$C_A^*(1/2)$, which is considered to originate from the same underlying mechanism. Unfortunately, this view is not accepted widely in the liquid crystal community. The existence of such additional subphases together with their superstructures must play an important role in clarifying the common origin in the underlying mechanism. As our notation suggests, three possible kinds of biaxial subphases are expected to exist: Sm$C_A^*(0 < q_T < 1/3)$, Sm$C_A^*(1/3 < q_T < 1/2)$ and Sm$C_A^*(1/2 < q_T < 1)$. Among these three, the existence of Sm$C_A^*(0 < q_T < 1/3)$ is now an indisputable fact (*54*, *55*); we give some additional evidence for its existence later. The presence is confirmed in several materials by three independent methods.

Although less adequately, Figure 2(f)–(i) and their expanded versions Figure 3(a)–(d), in particular, appear to indicate the emergence of an additional antiferroelectric subphase Sm$C_A^*(1/3 < q_T < 1/2)$, probably antiferroelectric Sm$C_A^*(2/5)$. The field-induced E–T phase diagrams show some characteristic closed loops of contour lines in the antiferroelectric SmC_A^* and Sm$C_A^*(1/2)$ temperature regions. Outside the loops and on the high-temperature side of Sm$C_A^*(1/3)$, there exists a reasonably wide temperature region, which can be assigned to the emergence of Sm$C_A^*(1/3 < q_T < 1/2)$; pay attention to the contour lines between 78.9 and 79.2°C in the 55 wt% mixture, between 76.0 and 76.6°C in the 60 wt% mixture, between 69.9 and 70.7°C in the 65 wt% mixture, and between 78.6 and 79.6°C in the 70 wt% mixture. We could not check the existence independently by observing the Bragg reflection due to the macroscopic helical structure, since the helical pitch is too long to give any reflection in the UV, visible or near-IR spectral region as expected (*63*, *64*). Although we did not perform any detailed conoscopic studies, it appears that conoscopy is not a powerful technique, either, in clarifying the emergence of Sm$C_A^*(1/3 < q_T < 1/2)$ in the binary mixture system under investigation. Moreover, some of the assignments previously made by observing field-induced conoscopic figures (*6*) might possibly misidentify the main range of Sm$C_A^*(1/2)$ as two independent subphases, since Figure 2(g)–(i) shows that the field-induced switching from Sm$C_A^*(1/2)$ occurs in complicated ways depending on the temperature as will be explained in detail in Section 3.2.

Regarding the existence of Sm$C_A^*(1/2 < q_T < 1)$, we can point out the closed contour loops observed at around 77.5°C in the 65 wt% mixture shown in Figure 2(h) and its expanded version Figure 4. It is not clear in this particular E–T phase diagram at the 65 wt% mixture whether any subphase really exists at $E = 0$, but

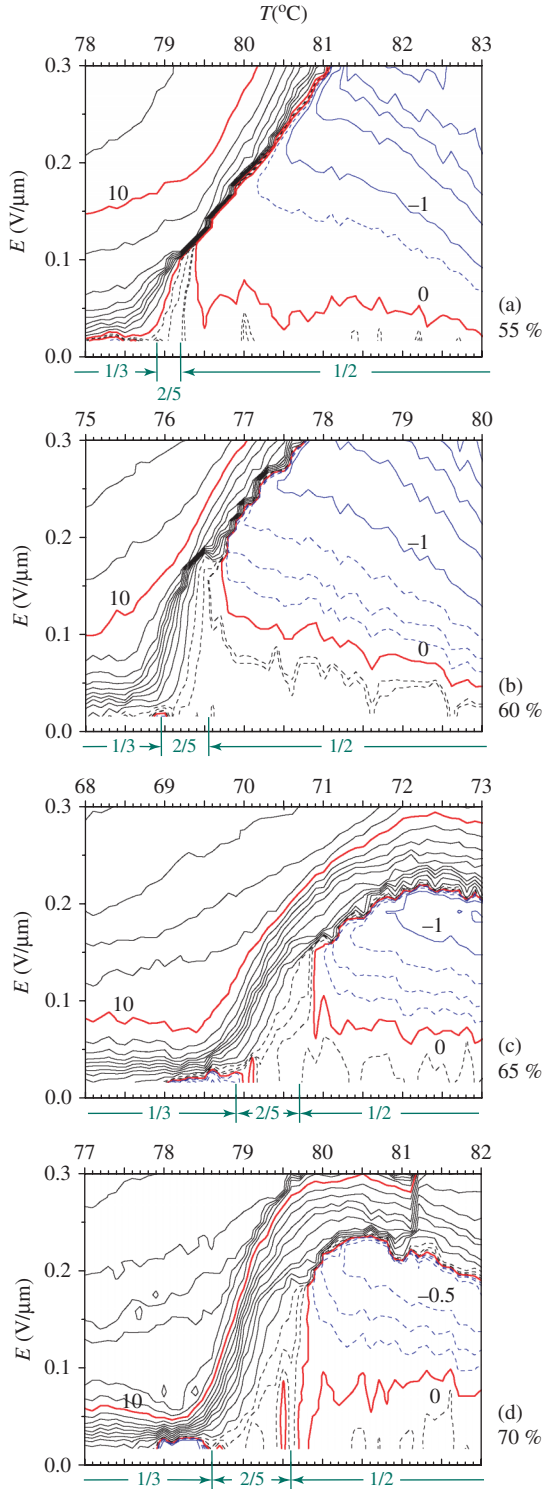

Figure 3. Expanded versions of Figure 2(f)–(i), indicating the existence of Sm$C_A^*(1/3 < q_T < 1/2)$, which is most probably Sm$C_A^*(2/5)$.

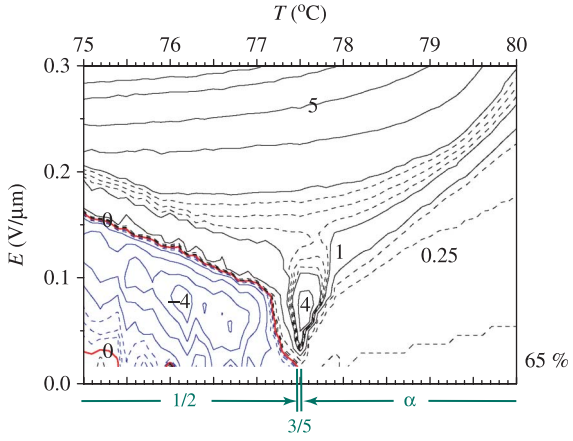

Figure 4. Expanded version of Figure 2(h). Birefringence contours are drawn by solid lines at an interval of $\Delta n = 1 \times 10^{-3}$; some auxiliary contours are given by dotted lines appropriately for convenience as a visual guide. Two kinds of closed contour loops are observed: negative, with the minimum of -4×10^{-3} in the Sm$C_A^*(1/2)$ temperature region; and positive, with the maximum of 4×10^{-3} between Sm$C_A^*(1/2)$ and SmC_α^*.

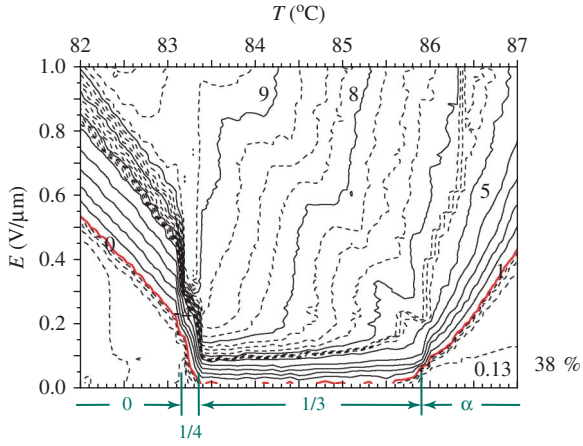

Figure 5. Expanded version of Figure 2(d), indicating the existence of Sm$C_A^*(1/4)$ conspicuously. Birefringence contours are drawn by solid lines at an interval of $\Delta n = 1 \times 10^{-3}$; some auxiliary contours are given by dotted lines appropriately for convenience as a visual guide.

some subphase certainly appears to be stabilised by slightly increasing the MHPOOCBC concentration. At first glance, it may be considered that this is the stabilisation of Sm*C** at $E = 0$. If this is so, why do we observe the closed contour loops? We ought to conclude that some subphase is to be stabilised at $E = 0$. It also seems to be related with the field-induced unwinding process of SmC_α^*. A much more detailed study on the MHPOOCBC concentration dependence at around 65 wt% may clarify the real cause of the closed contour loops. We would like to insist that the emergence of Sm$C_A^*(1/2 < q_T < 1)$ itself is well evidenced experimentally by the *E*–*T* phase diagrams shown in Figure 2(h) and its expanded version Figure 4.

The existence of Sm$C_A^*(0 < q_T < 1/3)$ has been observed in two ways, as a single subphase in the phase emerging sequences (1) and (2) or as several unstable subphases in the sequences (4) and (5). In the binary mixture system of (*S*)-12BIMF10 and (*S*)-MHPBC, Chandani *et al.* unambiguously proved the emergence of a single phase other than Sm$C_A^*(1/3)$ and Sm$C_A^*(1/2)$ and concluded on indirect evidence that this subphase must be antiferroelectric Sm$C_A^*(1/4)$ (see (*55*)). Although they did not confirm its superstructure with eight-layer periodicity by resonant X-ray scattering, the indirect evidence is not a trifling matter; remember that the three- and four-layer periodicities of the prototype subphases were concluded long before the confirmation by resonant X-ray scattering (*51*, *65*). In a binary (*S*)-MHPOCBC mixture containing 38 wt% (*S*)-MHPOOCBC, as reported in the previous paper (*53*) and reproduced in Figure 5, the similar subphase is confirmed to exist at between 83.15 and 83.35°C; the boundary between SmC_A^* and Sm$C_A^*(1/3)$ shows the two-step change indicating the existence of Sm$C_A^*(1/4)$. With increasing MHPOOCBC concentration, on the other hand, the boundary between SmC_A^* and Sm$C_A^*(1/3)$ looks increasingly broad, as seen clearly in Figure 2(i)–(l). In this boundary region, many birefringence contour lines are nearly vertical. Thus, the broader boundary must suggest the emergence of several unstable subphases.

In order to support this suggestion, we have studied the Bragg reflection spectra due to the helical structure of SmC_A^*. Figure 6 shows the reflection peak wavelength versus temperature for the 70 and 85 wt% mixtures. Both SmC_A^* and Sm*C** have the reflection peaks in the visible and near-IR wavelength regions. The handedness of the helix is just opposite to each other as usual (*64*(a), (b)), left-handed in SmC_A^* and right-handed in Sm*C**. The helical pitch of SmC_A^* becomes gradually shorter with increasing temperature, but it begins to increase rather suddenly when the temperature enters into the broad boundary region between SmC_A^* and Sm$C_A^*(1/3)$ as seen in Figure 6. At the same time the Bragg reflection spectra becomes weaker and broader rather suddenly as illustrated in Figure 7(a). The conspicuous broadening could not be explained by the pure and simple coexistence of SmC_A^* and Sm$C_A^*(1/3)$ due to the first-order phase transition between them. In this way we can conclude that the broad boundary results from the emergence of several unstable subphases. The similar conclusion has already been reported in 12OF1M7 by observing the

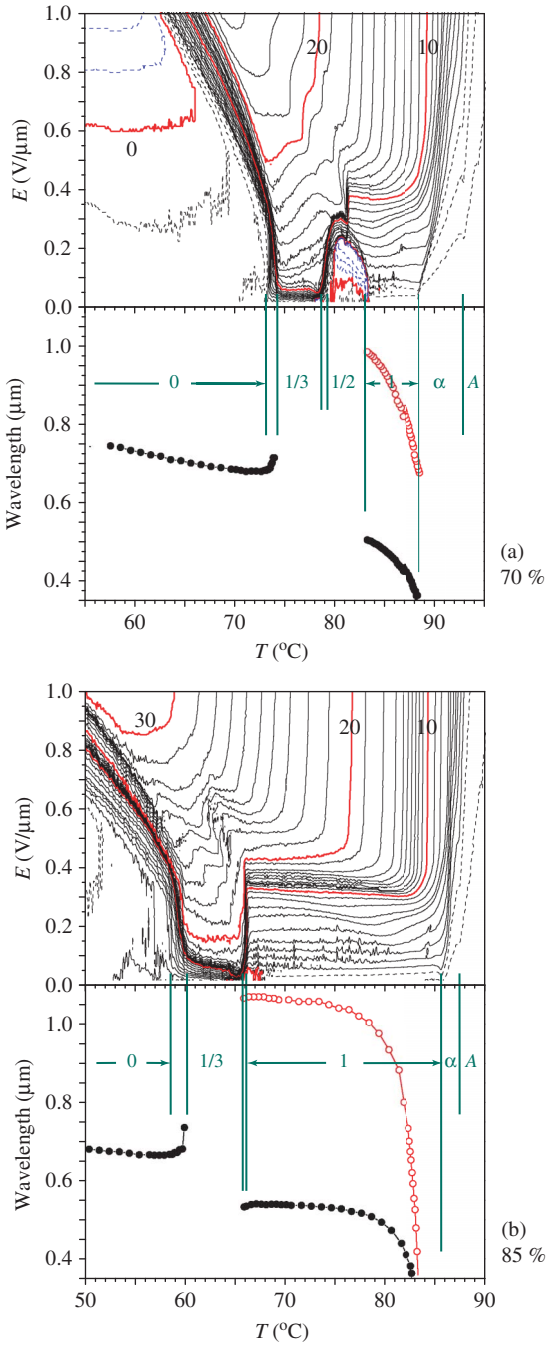

Figure 6. Comparison between E–T phase diagram and Bragg reflection peak versus temperature in MHPOCBC binary mixtures containing MHPOOCBC with (a) 70 wt% and (b) 85 wt% concentrations. The spectral peak becomes longer rather suddenly when the temperature enters into the boundary region between SmC_A^* and Sm$C_A^*(1/3)$; the Bragg reflection could not be observed in Sm$C_A^*(1/3)$.

multi-peaked characteristic reflection bands due to the modulated helical structures (*54*). The other high-temperature side boarder between Sm$C_A^*(1/3)$ and SmC^* seems also to be disturbed as shown in Figures 2(j)–(l) and 6, and the spectra becomes broader as illustrated in

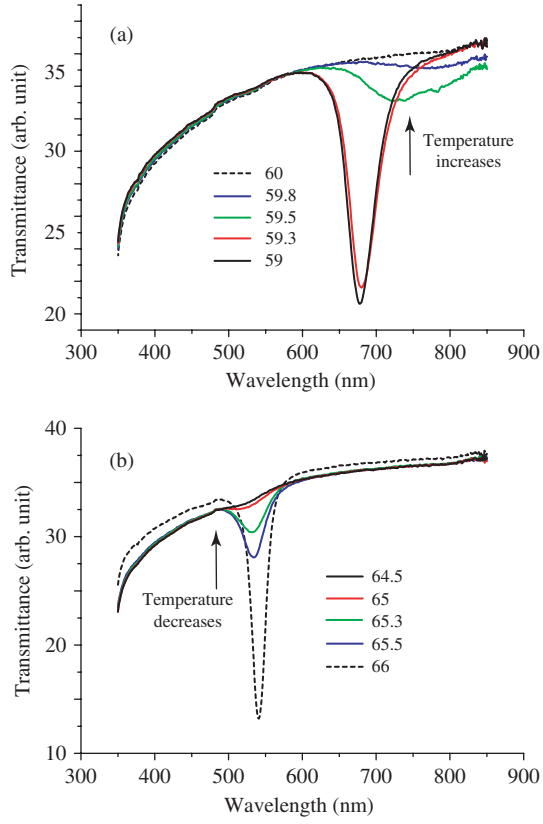

Figure 7. Brag reflection spectra in MHPOCBC binary mixture containing 85 wt% MHPOOCBC measured for a homeotropic cell of cell spacing 50 μm at an oblique incidence of 20°. The spectral width broadens rather suddenly when the temperature enters into the boundary regions between SmC_A^* and Sm$C_A^*(1/3)$.

Figure 7(b). This disturbance may suggest the emergence of some unstable subphases in the $1/3 < q_T < 1$ region in the subphase emergence sequence (5). The steep decrease of the SmC^* macroscopic helical pitch with rising temperature will be explained in detail later in Section 3.3.1.

3.1.2 Theoretical models predicting the emergence of biaxial subphases other than Sm$C_A^*(1/3)$ and Sm$C_A^*(1/2)$

We insist that the existence of some additional subphases other than the typical ones with superstructures consisting of three- and four-layer unit cells is experimentally established unambiguously. So far as we are aware of, four theoretical models have predicted such additional subphases (*14, 22, 26, 27, 66*). Yamshita and coworkers applied the ANNNI model and published a series of papers. Since the molecular orientational order parameter is as large as 0.7 or higher usually, it is hardly considered that thermal orientational fluctuations alone can produce the subphase superstructures; the ANNNI model Hamiltonian cannot be applied in

dealing with the frustration between SmC_A^* and SmC*. Both models considered by Dolganov *et al.* and by Hamanesh and Taylor predicted the subphase with superstructure consisting of a six-layer unit cell. Using the symmetry transformation properties of the general expression for the free energy of the corresponding subphases, Osipov and Gorkunov showed, without addressing a particular model, that there exist three possible six-layer unit cells (*67*). Since these cells have $q_T = 0$ or 2/3, a subphase with superstructure consisting of a six-layer unit cell, if any, must emerge in the region of $1/3 < q_T < 1$. For $q_T = m/n$ with even m or n, the subphase is antiferroelectric and its superstructure unit cell consists of $2n$ smectic layers; $q_T = 2/3$ has the unit cell consisting of six layers.

In this way the Emelyanenko–Osipov model alone can explain the observed additional subphases between SmC_A^* and Sm$C_A^*(1/3)$, i.e. Sm$C_A^*(0 < q_T < 1/3)$. In the temperature region of $0 < q_T < 1/3$, the Emelyanenko–Osipov model predicts the emergence of Sm$C_A^*(1/9)$, Sm$C_A^*(1/7)$, Sm$C_A^*(1/5)$ and Sm$C_A^*(1/4)$. Since their numerical calculations are restricted up to nine smectic layers, it is natural that Sm$C_A^*(1/8)$ and Sm$C_A^*(1/6)$, which have the unit cells of 16 and 12 layers, respectively, do not emerge in the subphase sequence Emelyanenko and Osipov obtained. They further studied the influence of the long-range interaction between polarisation fluctuations (*4*, *5*) and found that the most stable subphase other than typical Sm$C_A^*(1/3)$ and Sm$C_A^*(1/2)$ is Sm$C_A^*(1/4)$, which may change into a transition temperature region with rather unstable subphases. See Figure 5 of (*15*). The emergence of several unstable subphases must correspond to the broader boundary between SmC_A^* and Sm$C_A^*(1/3)$ as observed in Figure 2(i)–(l).

In the temperature region of $1/3 < q_T < 1/2$, possible subphases with rather simple superstructures are Sm$C_A^*(2/5)$ and Sm$C_A^*(3/7)$. In fact, their calculation suggests the emergence of Sm$C_A^*(3/7)$ (see (*55*)), but not that of Sm$C_A^*(2/5)$, since Sm$C_A^*(2/5)$ has the unit cell of 10 layers; note that their numerical calculations were performed by taking into account the subphase superstructures with unit cells consisting of up to nine smectic layers. Since Sm$C_A^*(2/5)$ and Sm$C_A^*(3/7)$ are antiferroelectric and *ferrielectric*, respectively, however, the actually observed subphase must be Sm$C_A^*(2/5)$. It should be noted that, in the global evolution of the *E*-*T* phase diagram, the antiferroelectric subphase emerges from the zero field side while the *ferrielectric* subphase comes to exist stably from the high field side. In particular, the existence of the subphase Sm$C_A^*(1/3 < q_T < 1/2)$ is recognised as some peculiarities on the low-temperature side of antiferroelectric Sm$C_A^*(1/2)$ in the *E*-*T* phase diagrams shown in Figure 2(f)–(i) and their expanded versions Figure 3(a)–(d).

Regarding Sm$C_A^*(1/2 < q_T < 1)$, the closed loops of contour lines observed at around 77.5°C in Figure 2(h) and its expanded version Figure 4 are quite intriguing. Two of the simplest possible subphases are *ferrielectric* Sm$C_A^*(3/5)$ and antiferroelectric Sm$C_A^*(2/3)$, which have superstructures with five- and six-layer periodicities, respectively. The apparently simple similar subphases, Sm$C_A^*(3/4)$ and Sm$C_A^*(4/5)$, are both antiferroelectric and their superstructures with eight-and ten-layer periodicities are slightly more complicated. As pointed out above, both models considered by Dolganov *et al.* and by Hamanesh and Taylor predict antiferroelectric Sm$C_A^*(2/3)$. The subphase related with the closed contour loops under consideration does not seem to be antiferroelectric, however, since it is going to be stabilised from the high field side. Moreover since Figure 2(h) and its expanded version Figure 4 indicate that it is also related with the unwinding process of SmC_α^*, the most probable candidate must be *ferrielectric* Sm$C_A^*(3/5)$, which has the microscopic short-pitch helical structure with a periodicity of one turn by five layers. See Figure 3(a) of (*67*). Recently, Yamashita's group in Mie University studied the field-induced unwinding process of SmC_α^* and found that its short-pitch helical structures with periodicities of one turn by three, four and five layers, i.e. $p_\alpha = 3$, 4 and 5, play a critical role (*41*–*44*). The relation between SmC_α^* with $p_\alpha = 5$ and Sm$C_A^*(3/5)$ is expected to be similar to the relation between SmC_α^* with $p_\alpha = 3$ and Sm$C_A^*(1/3)$, as will be discussed in detail in Section 3.3.2.

As stated above, the biaxial subphase Sm$C_A^*(q_T)$ has a microscopic short-pitch helical structure, although highly distorted. In the Emelyanenko–Osipov model, the pitch is generally given by

$$|p_{qT}| = \frac{2}{1 - q_T}, \tag{3}$$

in the unit of the number of smectic layers, and the handedness is determined by the sign of $c_p c_f$, where c_p and c_f are the coefficients giving the piezoelectric (ordinary spontaneous) and flexoelectric polarisations, respectively. In the (*S*)-MHPOCBC–(*S*)-MHPOOCBC binary mixture system we studied here, the biaxial subphases can be concluded to have the right-handed microscopic short-pitch helical structure, because of the following three reasons: (i) the helix is right-handed in SmC* of this binary mixture system as experimentally confirmed above; (ii) sometimes the helical structure continuously changes from

SmC* to SmC^*_α (see (*13*, *35*, *54*)) as we also experimentally confirmed below; and (iii) the evolution of *E*–*T* phase diagrams in this binary mixture system clearly indicates that SmC^*_α and unwound Sm$C^*_A(1/3)$ are closely related (*53*).

To be precise, the microscopic short-pitch helical structure of the biaxial subphases approximately given by Equation (3) is not commensurate with the smectic layer, since the biaxial subphases also have the macroscopic long-pitch helical structure. Empirically, the macroscopic pitch is approximately given by

$$\frac{1}{p(\mathrm{Sm}C^*_A(q_T))} = \frac{q_T}{p(\mathrm{Sm}C^*)} + \frac{1-q_T}{p(\mathrm{Sm}C^*_A)}, \qquad (4)$$

where the helical pitch p is considered to be positive for the right-handed helix and negative for the left-handed helix. Since the handedness of the macroscopic helical structure in Sm*C** is just opposite to that in SmC^*_A (see (*64*(a), *64*(b))), the macroscopic pitch is usually rather long in Sm$C^*_A(1/3)$ and Sm$C^*_A(1/2)$. Moreover, Sm$C^*_A(1/3)$ has its intrinsic instability and hence the macroscopic helical structure may be disturbed dynamically as well as statically (*22*, *52*). Detailed theoretical calculations for the macroscopic pitch were also reported (*63*).

Before closing Section 3.1.2, it is worthwhile reconsidering the fundamental premise that SmC^*_A is the low-temperature main phase of Sm*C**. Using q_T in designating the subphases fundamentally depends on the premise. However, the extraordinary variety of intermoleculer interactions sometimes makes it possible to stabilise Sm*C** absolutely at lower temperatures instead of SmC^*_A. An intriguing example recently reported is the binary mixture system of antiferroelectric MC881 and ferroelectric MC452, where the boundary between SmC^*_A and Sm*C** in the temperature-concentration phase diagram appears nearly vertical and parallel to the temperature axis; hence, SmC^*_A could not exist as a low-temperature phase of Sm*C** on the ferroelectric side of the boundary (*68*). In such a case, using q_T is still possible, but the way of subphase emergence in the critical concentration region may be affected largely. Much more impressive is the reentrant emergence of Sm*C** on the low-temperature side of SmC^*_A reported by Pociecha *et al.* (*69*); they were very careful to confirm that this reentrant Sm*C** phase is different from the ferroelectric hexatic phase. In contrast to the ordinary case, therefore, the lower-temperature subphase is expected to have a *larger* q_T than the higher-temperature subphase, if any subphases emerge between reentrant Sm*C** and SmC^*_A. The most surprising result is the phase sequence reversal confirmed by resonant X-ray scattering, where the antiferroelectric phase with superstructure consisting of a four-layer unit cell emerges on the high-temperature side of Sm*C** (see (*70*, *71*)). We hesitate to designate this as Sm$C^*_A(1/2)$, because it gains stability over a range of almost 40°C and could not be considered as a subphase.

3.2 *Field-induced deformation and resulting stable states of biaxial subphases*

When the applied electric field is sufficiently high, all of the main phases and sub-phases under consideration may become completely unwound Sm*C**. Actually, the maximum field we applied in this study, 1 V μm^{-1}, is not high enough to realise completely unwound Sm*C** in many of them. However, Sm*C** itself can easily be unwound completely and birefringence contours are vertical and, hence, parallel to the ordinate field E axis as obviously seen in Figure 2(i)–(1). This means that the electroclinic effect is small in completely unwound Sm*C** and that the director tilt angle Θ is determined mainly by T and almost independent of E. In contrast, the electroclinic effect plays an important role in Sm*A*, and the birefringence contours are actually oblique as also seen in Figure 2(i)–(1). The unwinding process of SmC^*_α is studied in detail in Section 3.3.2. The unwinding of SmC^*_A macroscopic helical structure was once considered to arise initially from the interaction of the electric field with the dielectric anisotropy or residual polarisation (*72*–*75*). Actually, however, the mechanism for helix distortion is the interaction between the electric field and induced polarisation. This is caused by a perturbation to the anticlinic ordering. The induced polarisation interacts with the applied field to rotate the **c** directors to align with the field, and eventually causes helix unwinding (*72*, *76*); consequently the field-induced birefringence may become negative as explicitly observed in some of Figure 2(a)–(1).

The helix unwinding in Sm$C^*_A(1/2)$ occurs similarly, and is completed at rather low fields since the pitch is usually very long (*9*, *52*); the field-induced birefringence becomes negative as clearly seen in Figure 2(f)–(i) and their expanded versions Figure 3(a)–(d). The way Sm$C^*_A(1/2)$ changes into completely unwound Sm*C** is complicated. Shtykov *et al.* showed the different behaviour of Sm$C^*_A(1/2)$ in the low-and high-temperature regions; its field-induced phase transition first occurs to Sm$C^*_A(1/3)$ and then to Sm*C** in the low-temperature region, while it occurs directly to Sm*C** in the high-temperature region although they split Sm*C** into FiLC and Sm*C** at that time (*77*). Manjuladevi and Vij have recently shown that FiLC differs from Sm*C** in only the magnitude of the helical pitch (*78*). At zero field FiLC has a longer pitch than Sm*C** which has relatively short pitch. The similar field-induced transition from Sm$C^*_A(1/2)$ to Sm$C^*_A(1/3)$ was also reported in the early stage of the subphase investigations (*6*). Quite

recently, Jaradat *et al.* confirmed using resonant X-ray scattering that Sm$C_A^*(1/2)$ undergoes a transition either to Sm$C_A^*(1/3)$ or to SmC*, depending on temperature (*79*). They remarked that the field-induced transition from Sm$C_A^*(1/2)$ to Sm$C_A^*(1/3)$ was surprising, because the four-layer polar structure proposed by Osipov and Gorkunov (*67*) was considered to be the more intuitive possibility than the three-layer polar Sm$C_A^*(1/3)$ structure, as suggested by Marcerou *et al.* (*80*) who studied a similar system without the benefit of resonant X-ray scattering. Whether it is surprising or not appears to be a highly controversial question; in fact, the field-induced deformation of Sm$C_A^*(1/2)$ toward unwound SmC* is quite dependent of the material and temperature as seen in Figure 2(e)–(i).

So let us first look at a supposedly much simpler case, i.e. the field-induced deformation of Sm$C_A^*(1/3)$. Hiraoka *et al.* (*48*) measured the apparent tilt angle as a function of applied field in a homogeneous cell of prototype MHPOBC (*2*). They observed, in the Sm$C_A^*(1/3)$ temperature region, that the apparent tilt angle increases considerably without showing any threshold in a low field region of less than about 0.1 V μm^{-1} due to the helix unwinding process, attains the plateau of unwound Sm$C_A^*(1/3)$ with an apparent tilt angle of about 1/3 of the SmC* tilt angle which extends over about 0.6 V μm^{-1}, and then shows an increase again indicating the field-induced phase transition from unwound Sm$C_A^*(1/3)$ to unwound SmC*. Recently, the similar unwinding process of Sm$C_A^*(1/3)$ and its stable unwound state followed by the field-induced transition to unwound SmC* are also confirmed by resonant X-ray scattering in another material (*79*). The stable existence of field-induced unwound Sm$C_A^*(1/3)$ appears to have been widely accepted. At the same time, it is quite natural to consider that, if the subphase itself is not really stable, unwound Sm$C_A^*(1/3)$ may not emerge as the plateau of the apparent tilt angle or the vertical contour lines of the field-induced birefringence. In fact, partial racemisation surely reduces the stability and makes it difficult to observe unwound Sm$C_A^*(1/3)$ as the vertical contour lines, which is clearly seen in nominally optically pure MHPBC (*55*).

The rather systematic data here obtained and shown in Figure 2(d)–(l) indicate that the field-induced transition from Sm$C_A^*(1/3)$ to unwound SmC* is also very intriguing. It may occur at multiple steps but not at a single step. In Figure 2(d), we can see that some of the contour lines have at least two vertical parts before reaching unwound SmC*; the lowest part apparently indicates unwound Sm$C_A^*(1/3)$. This is much more clearly visible in its expanded version Figure 5, although the contour lines are very noisy because the temperature axis is greatly expanded to show the existence of Sm$C_A^*(0 < q_T < 1/3)$ unambiguously. As the MHPOOCBC concentration increases, the lowest vertical part moves toward the slightly higher field side, becoming blurred, and almost disappears in Figure 2(g). The vertical part emerges again at rather high field region in Figure 2(h), which may or may not be unwound Sm$C_A^*(1/3)$. In Figure 2(i), the transition from Sm$C_A^*(1/3)$ to unwound SmC* may occur via the two vertical parts corresponding to the field-induced stable states, which are apparently closely related with the sigmoid type contour lines observed in the Sm$C_A^*(1/2)$ temperature region. The sigmoid type contour lines can be seen even in the Sm$C_A^*(1/3)$ temperature region in Figure 2(j) and (k). This means that the field-induced birefringence at a constant temperature may temporarily decrease with increasing applied field.

In this way it now becomes clear that the field-induced transition from Sm$C_A^*(1/3)$ to unwound SmC* can also have the staircase character. Increasing the applied electric field produces nearly the same effect as increasing the temperature in the sense that both favour the ferroelectric state. Similar situations are realised: the dominant ordering forces favouring anticlinic antiferroelectricity and synclinic ferroelectricity are nearly equal and a large number of subphase superstructures must have nearly the same free energy (*4*, *5*). Since the applied field selectively chooses the director tilting sense, the q_T number introduced in Section 1 is not suitable to use. Instead the number

$$q_E = \frac{|[R] - [L]|}{[R] + [L]}, \tag{5}$$

must work appropriately, where $[R]$ and $[L]$ refer to the numbers of smectic layers with directors tilted to the right and to the left, respectively, in a unit cell of the superstructure (*6*). It is natural to anticipate that the same long-range interlayer interaction forces proposed by Emelyanenko and Osipov (*14*) are operative, and hence a series of superstructures specified by q_E must be stabilised during the field-induced transition from the biaxial subphases as well as the SmC_A^* main phase to unwound SmC*. All of the antiferroelectric phases, SmC_A^*, Sm$C_A^*(1/4)$ and Sm$C_A^*(1/2)$, must have $q_E = 0$ at zero field, whereas *ferrielectric* unwound Sm$C_A^*(1/3)$ and ferroelectric unwound SmC* must have $q_E = 1/3$ and $q_E = 1$, respectively. The long-range interlayer interaction forces are usually weak, and hence q_E may increase monotonically with increasing applied field.

Some of the simple, possibly stable states with $q_E = 1/5, 1/3, 1/2$ and $3/5$ are expected to appear during the field-induced transition. Since Sm$C_A^*(1/3)$ has $q_E = 1/3$, it is reasonable to consider the two steps on

the Δn = 8–9 × 10^{-3} contour lines in Figure 2(d) and Figure 5 as the field-induced stable states with q_E = 1/3 and 1/2; note that the field not only unwinds the helical structure but also stabilises the intrinsic instability of Sm$C_A^*(1/3)$ (see (*22*, *52*)). In Figure 2(i) where the vertical parts of the contour lines appear in the more than about 0.5 V μm^{-1} field region, on the other hand, it is not impertinent to consider that Sm$C_A^*(1/3)$ changes into the stable q_E = 1/2 state without passing stable unwound Sm$C_A^*(1/3)$ with q_E = 1/3. Since we can clearly see the two steps on the Δn = 19 × 10^{-3} contour line in Figure 2(i), the transition from Sm$C_A^*(1/3)$ to unwound Sm*C** may occur via the two field-induced stable states with q_E = 1/2 and 3/5. It is worthwhile noting that the four- and five-layer polar superstructures proposed by Osipov and Gorkunov have q_E = 1/2 and 1/5, respectively. See Figures 2(a) and 3(b) of (*67*); q_E = 3/5 does not emerge because they do not take into account of any applied electric field effect. These field-induced stable states have the Ising-like structure with the largely distorted short-pitch helical structure. The distortion from the planar structure is not so large that the spontaneous polarisation of each state can be estimated from the value in Sm*C** at the same temperature. Therefore, we may be able to determine the q_E numbers of the field-induced stable states by observing the cell voltage with time under a constant current as Marcerou *et al.* did recently (*80*).

Now let us revert to the field-induced transition from the antiferroelectric subphase, Sm$C_A^*(1/2)$, to unwound Sm*C**. In the beginning it is worthwhile to note that the field-induced transition from the antiferroelectric main phase, SmC_A^*, to unwound Sm*C** occurs directly or via stable unwound Sm$C_A^*(1/3)$ (see (*81*)). As seen in Figure 2(i), where Sm*C** emerges on the high-temperature side of Sm$C_A^*(1/2)$, the direct transition to unwound Sm*C** is observed in the high-temperature region of Sm$C_A^*(1/2)$. Even when SmC_α^* adjoins Sm$C_A^*(1/2)$, the direct transition seems to be observed similarly as in Figure 2(g). The vertical part of the contour lines in the low-temperature region of Sm$C_A^*(1/2)$ of Figure 2(f) and (g) may indicate stable unwound Sm$C_A^*(1/3)$ with q_E = 1/3, which Jaradat *et al.* and Marcerou *et al.* (*79*, *80*) reported to emerge in other materials. In Figure 2(g), however, the emergence of stable unwound Sm$C_A^*(1/3)$ with q_E = 1/3 is slightly questionable; as pointed out in the preceding paragraphs the stability decreases with increasing MHPOOCBC concentration from Figure 2(d) to (i) and, hence, the vertical part may possibly indicate stable q_E = 1/2, which is the aforementioned four-layer polar structure proposed by Osipov and Gorkunov (*67*) and considered to be the more intuitive possibility than the three-layer polar structure, i.e. unwound Sm$C_A^*(1/3)$ with q_E = 1/3 by Jaradat *et al.* and Marcerou *et al.* (*79*, *80*). In fact, the field-induced transition from Sm$C_A^*(1/2)$ to a stable state with q_E other than 1/3, possibly to stable q_E = 1/2, appears to occur in Figure 2(h).

The sigmoid-type contour lines observed in Figure 2(i)–(k) indicate, as already pointed out above, that the field-induced birefringence at a constant temperature may temporarily decrease with increasing applied field. This can be understood by assuming that various field-induced states emerge sequentially in a rather narrow field strength range and that some of them have superstructures with large unit cells. Suppose that the field-induced transition in Figure 2(i) occurs from Sm$C_A^*(1/2)$ with q_E = 0 to stable q_E = 3/5, several possible metastable states with q_E = 0, 1/9, 1/7,1/5,1/4, 1/3, 3/7, 1/2 and 5/9 may emerge sequentially between them. Note that we take into account superstructures with unit cells up to nine smectic layers. Since the same long-range interlayer interaction forces must be operative in the field-induced phase transition, stable states with large unit cells are considered to have small biaxiality. See the numerically calculated results for subphases in the temperature-induced phase transition given in Figure 4 of (*14*). Likewise there are many possible states between q_E = 3/5 and unwound Sm*C** with q_E = 1. These series of states may be responsible for the characteristic shape of contour lines observed in the Sm$C_A^*(1/3)$ temperature range shown in Figure 2(j) and (k). The closed loops of contour lines observed at around 77.5°C in Figure 2(h) and its expanded version Figure 4 also indicate that the field-induced birefringene at a constant temperature may temporarily decrease with increasing applied field. This is understandable on the basis of ferrielectric Sm$C_A^*(3/5)$ with q_E = 1/5 stabilised at E = 0 in a narrow temperature range; the field-induced transition to unwound Sm*C** with q_E = 1 may occur via several metastable states, some of which must have smaller biaxiality than Sm$C_A^*(3/5)$. We need much more detailed investigations, both experimentally and theoretically, to clarify the characteristic staircase features in these interesting frustration phenomena in tilted smectic liquid crystals. In particular, no detailed calculations based on the Emelyanenko–Osipov model have yet been performed for the electric-field-induced phase transition.

3.3 Evolution of SmC_α^* short-pitch helical structure and its field-induced unwinding

3.3.1 Temperature variation of short-pitch helical structure and global phase emerging sequence

When optically uniaxial SmC_α^* does appear, on its high-temperature side it always borders Sm*A*, whereas on

its low-temperature side, SmC^*_α adjoins one of the several phases, SmC^*_A, Sm$C^*_A(0 < q_T < 1/3)$, Sm$C^*_A(1/3)$, Sm$C^*_A(1/2)$ and SmC*. The emergence of Sm$C^*_A(0 < q_T < 1/3)$ directly below SmC^*_α is only confirmed in 12BIMF10, where this subphase is considered to be Sm$C^*_A(1/4)$ (see (*55*)). It is experimentally well established, as stated in Section 1, that SmC^*_α has the microscopic helical structure with a short pitch, p_α, which changes continuously with temperature and is usually measured as the number of smectic layers in one turn, although not commensurate with the smectic layer (*7, 8, 29–39*). In the extended Emelyanenko–Osipov model (*16*, *63*), the emergence of SmC^*_α is ascribed to degeneracy lifting at the frustration point, where the three main phases, SmC^*_A, SmC* and SmA, happen to have the same free energy. The lifting is caused by the effective long-range interlayer interaction forces, which result from the minimisation of free energy with respect to the in-layer polarisation and produce the couplings between the director orientations in separated smectic layers. The presence of the discrete flexoelectric polarisation (*14, 17, 18, 23, 55*) which is not parallel to the ordinary chirality-induced, piezoelectric polarisation causes the short-pitch helical structure with such large twist, although only the polarization–polarisation interactions between adjacent smectic layers are taken into account. This is an intriguing idea if we reflect that almost all intermolecular interactions favour the planar structure, except for the weak chiral interaction responsible for the macroscopic helical structure with a long pitch of micrometre scale. Shtykov *et al.* (*16*) and Emelyanenko *et al.* (*63*) obtained the phase diagrams numerically by taking into account of commensurate short pitches with periodicities of up to nine smectic layers.

Their $d^4/V_{\mathrm{eff}} - \tilde{T}$ phase diagrams calculated for several $c_\mathrm{f}/c_\mathrm{p}$ values and shown in Figure 9 of (*16*) approximately reproduce the evolution of phase sequences (1)–(6) described in Section 3.1.1. Here d^4/V_{eff} can be regarded as the ratio of relative strength of antiferroelectricity versus ferroelectricity, and $c_\mathrm{f}/c_\mathrm{p}$ is the ratio between the discrete flexoelectric and the ordinary piezoelectric constants producing the corresponding spontaneous polarisations. The phase diagrams also predict, to some extent, whether p_α becomes shorter or longer with increasing temperature depending mainly on the d^4/V_{eff} value. When it is sufficiently large, SmC^*_α directly adjoins SmC^*_A on the low-temperature side as in the phase sequence (1), and p_α monotonically increases with rising temperature. The first-order phase transition always occurs between SmC^*_A and SmC^*_α experimentally. In the extended Emelyanenko–Osipov model, however, no phase transition occurs and the SmC^*_A macroscopic helical structure changes into the SmC^*_α microscopic helical structure continuously. Note that the handedness of the macroscopic helix is opposite to that of the microscopic helix. When it becomes slightly smaller and $c_\mathrm{f}/c_\mathrm{p}$ is rather small, however, the temperature variation of p_α may abruptly change from increasing to decreasing when the system crosses the synclinic–anticlinic boundary. This abrupt change was once considered as a cause of the SmC^*_α structure in MHPOCBC that consists of high- and low-temperature parts (*16*). However another possible explanation was given recently (*53*) and hence it is not clear so far whether the abrupt change occurs in actual compounds and mixtures. The monotonic increase of p_α in MHPOCBC was experimentally confirmed by Cady *et al.* (*38*) Apparently, however, the high-temperature part did not seem to be observed in their measurements using thin free-standing films (*16*).

When d^4/V_{eff} is sufficiently small, on the other hand, SmC^*_α directly adjoins SmC* on the low-temperature side as in the phase sequences (5) and (6), and p_α decreases monotonically with rising temperature. When it becomes slightly larger and the phase sequence is given by (4), however, p_α may increase monotonically with rising temperature. Consequently, both cases of increasing and decreasing p_α are possible in SmC^*_α emerging on the high-temperature side of SmC*. In fact, the increasing and decreasing cases are confirmed in 10OTBBB1M7 by Mach *et al.* (*7*, *8*) and in 11HFBBM7 by Schlauf and Bahr (*30*), respectively. The E–T phase diagrams given in Figures 2(i)–(l) and 6(a) and (b) show the characteristic evolution of SmC^*_α directly adjoined SmC* on the low-temperature side. As the MHPOOCBC concentration increases, the temperature range of SmC^*_α becomes narrower while that of SmC* widens. In Figure 2(i) and Figure 6(a), SmC* and SmC^*_α emerge in the temperature ranges of 83.0–88.4°C and 88.4–92.8°C, respectively, and the phase boundary between them can be seen clearly. In Figure 2(j) and Figure 6(b), the boundary becomes less clear but is still identified by dents of contour lines at 85.7°C; the temperature ranges of SmC* and SmC^*_α are 66.1–85.7°C and 85.7–87.4°C, respectively.

The macroscopic helical pitch of SmC* decreases sharply with increasing temperature and the Bragg reflections become buried in the intrinsic absorption in Figure 6(b); it does not seem to change into the microscopic helical structure of SmC^*_α continuously, however, since the boundary can be seen as the dents of contour lines as pointed out above. In Figure 6(a), the Bragg reflections observed in the visible wavelength region suddenly disappear at the phase transition to SmC^*_α, where p_α must keep decreasing with rising temperature, as actually confirmed by Schlauf and Bahr (*30*) in 11HFBBM7. When the MHPOOCBC concentration further increases, the change from SmC*

to SmC^*_α becomes gradually smoother, and in Figure 2(1) as well as in pure MHPOOCBC (not shown) the macroscopic helical pitch of Sm*C** may continuously change into the microscopic helical pitch of SmC^*_α. Cady *et al.* (*37*) confirmed this sort of continuous change from macroscopic to microscopic in 11OHFBBB1M7 by ellipsometry and concluded that the helical pitch changes from around 70 smectic layers, which gives the characteristic reflection band (the half-pitch band) at about 370 nm and the full-pitch band at about 740 nm, to about 15 smectic layers. Da Cruz *et al.* (*35*) also noted, by studying their homologous series compounds using differential scanning calorimetry (DSC) and optical measurements, that the change of the helical pitch from Sm*C** to SmC^*_α may occur discontinuously or continuously. Since both Sm*C** and SmC^*_α have the same symmetry, the phase transition should be a first-order transition, which ends at a critical point; beyond the critical point, the change occurs continuously and no phase transition is observed.

In this way, the $d^4/V_{\text{eff}} - \tilde{T}$ phase diagrams obtained numerically on the basis of the simply extended Emelyanenko–Osipov model (*16*) can, on the whole, explain the experimentally observed temperature variation of the SmC^*_α short helical pitch, p_α, which characteristically depends on the phase emerging sequences (1)–(6) given in Section 3.1.1. If we consider the sequences (1) and (6) only by disregarding the emergence of any biaxial subphases but still by taking the emergence of uniaxial SmC^*_α for granted, we can analytically obtain the polarisation-dependent part of the free energy used in (*16*) which is responsible for the emergence of SmC^*_α as given in Appendix 1. The total free energy thus analytically obtained can easily explain the experimentally observed strong contrast between the short-pitch helical structure observed just above SmC^*_A and that emerging just above Sm*C**; in the former case the short-pitch becomes longer up to 4, while in the latter case it becomes shorter at most 20 or slightly less but never to 4 or less (*30*, *38*, *53*). Furthermore, the analysis indicates that the short-pitch helical structure would not emerge if the positional correlation between adjacent layers g is larger than 0.5. It is intriguing that g should be reasonably small but not too small; such a situation is just realised in smectic mesophases with fluid layers. It is worthwhile noting that the right-handed short-pitch helical structure corresponds to $c_p c_f < 0$.

The total free energy never shows two minima separated by a barrier between $\Delta\varphi = \pm 90°$ and 0° or $\Delta\varphi = \pm 90°$ and ±180°; it always predicts the continuous change from SmC^*_α to SmC^*_A or Sm*C**. In the more sophisticated version (*63*), the discontinuous change experimentally observed is explained by the presence of the biaxial ordering of the molecular short axis. Since the biaxial ordering should occur in Sm*A* in that explanation, however, it is hardly acceptable from an experimental point of view to consider the biaxial ordering as a cause of the discontinuous change, i.e. the occurrence of the phase transition from SmC^*_α to SmC^*_A or SmC^*. The biaxial ordering must play an important role at lower temperatures where the director tilt is large (*82*) but not in Sm*A*. We have to look for any other cause of discontinuous change on the low-temperature side but not on the high-temperature side toward Sm*A*. We suspect that the elastic energy for the large twist in SmC^*_α critically depends on the director tilt angle and may cause the first-order transition observed experimentally.

3.3.2 Unwinding process as the condensation of discrete solitons

The fundamental issue is how to make a compromise between the short-pitch helical structure of SmC^*_α and its staircase character observed in the response to an applied electric field (*6, 47–49*). The conspicuous observation was made most recently in the *E–T* phase diagram of MHPOCBC that SmC^*_α consists of high- and low-temperature parts (*16*). In the previous paper (*53*), we discussed the origin and structures of these two parts in terms of the extended Emelyanenko–Osipov model together with the devil's staircase character of the field-induced unwinding process of the short-pitch helical structure (*16, 41–46*). Irrespective of the actual occurrence of a sudden change in p_α from increasing to decreasing at a temperature within SmC^*_α as considered in (*16*), the applied field may deform the short-pitch helical structure characteristically depending on p_α at $E = 0$, producing the apparent high- and low-temperature parts. The *E–T* phase diagrams in the low MHPOOCBC concentration region, i.e. for 0, 12, 25 and 38 wt% shown in Figure 2(a)–(d), allowed us to conclude as follows.

(1) The applied electric field distorts the low-temperature part of SmC^*_α toward distorted Sm$C^*_A(1/3)$ coming down in the lower field region.
(2) The border between the low- and high-temperature parts of SmC^*_α in MHPOCBC must correspond to $p_\alpha = 3$.
(3) It moves toward SmC^*_A with increasing MHPOOCBC concentration.
(4) Once it reaches SmC^*_A, Sm$C^*_A(1/3)$ simultaneously touches the abscissa temperature axis and comes to exist even at $E = 0$.

Now let us move to the *E–T* phase diagrams in the medium MHPOOCBC concentration region. In

Figure 2(d), SmC^*_α looks structureless and may correspond to the high-temperature part mentioned above and in the previous paper (*53*). In Figure 2(e) and (f), however, SmC^*_α comes to show conspicuous structures again.

The phase diagrams numerically obtained using the extended Emelyanenko–Osipov model and given in Figure 9 of (*16*) seem to suggest that p_α may always increase with rising temperature when SmC^*_α is adjacent to Sm$C^*_A(1/3)$ as in the phase sequence (2) given in Section 3.1.1. When SmC^*_α borders on Sm$C^*_A(1/2)$ as in the phase sequence (3), it is not easy to predict precisely whether p_α increases or decreases and both seem to be possible. Recently, Liu *et al.* (*39*) studied the binary mixture system of *R*-10OTBBB1M7 and *R*-MHPOCBC and determined p_α for several mixtures. In particular, Table I in their paper is very informative and suggestive, showing that p_α always increases with rising temperature for all of the phase sequences (1), (2) and (3); p_α ranges between 3.35 and 4.45 smectic layers for the phase sequence (2) and between 3.65 and 7.7 smectic layers for the phase sequence (3). Since there are no such detailed data for p_α in the MHPOCBC–MHPOOCBC mixture system under study in this paper, we simply assume the similar temperature variation of p_α as will be discussed below.

Quite recently, Yamashita's group in Mie University (*41–43*) theoretically studied the electric-field-induced phase transition from SmC^*_α to SmC (unwound SmC*), i.e. the unwinding process of SmC^*_α, as a condensation process of discrete solitons (*44*). They found that the process exhibits a devils staircase for $p_\alpha > 4$, that $p_\alpha = 3$ tends to keep the three-layer structure, and that the unwinding process appears to occur toward SmC_A (unwound SmC^*_A) for $p_\alpha < 3$. For $4 > p_\alpha > 3$, the unwinding process of SmC^*_α appears to show the devil's staircase character but many more studies are needed to elucidate the details. The relations between soliton lattice period and applied electric field for $p_\alpha > 3$ are not continuous smooth curves but show the devil's staircase structures as illustrated in Figure 2 of (*42*); stairs with soliton lattice periods of 4, 13/3, 9/2, 5 appear to be rather stable. Since the soliton lattice period at $E = 0$ is p_α and is expected to range between 3.65 and 7.7 smectic layers for the phase sequence (3) as stated above, it is reasonable to consider that some of the rather stable soliton lattice periods of 4, 13/3, 9/2 and 5 must be responsible for the characteristic deformation observed in Figure 2(e) and (f). In order to make a detailed comparison between theory and experiment, however, we need to obtain more experimental data and to remove the crucial assumptions used in the theoretical treatments. Their numerical calculations were performed on the unrealistic assumption of the constant tilt angle and by disregarding the important role played by the long-range interlayer interaction forces.

During the subphase evolution with increasing MHPOOCBC concentration shown in Figure 2(a)–(d), we can see the characteristic relation between SmC^*_α and Sm$C^*_A(1/3)$ as pointed out above. A special role is played by SmC^*_α with p_α=3, i.e. α_3; the temperature at which Sm$C^*_A(1/3)$ comes to exist at $E = 0$ in a particular material corresponds to the temperature where SmC^*_α has the short helical pitch of p_α=3 smectic layers. It is not only the long-range interlayer interaction forces introduced by Emelyanenko and Osipov (*14*) but also the condensation process of discrete solitons studied by Yamashita's group in Mie University (*41–44*) that stabilise the superstructure with a unit cell of three-layer periodicity. In other words, Sm$C^*_A(1/3)$ at $E = 0$ not only has the macroscopic long-pitch helical structure but also the short-pitch helical structure of one turn by three layers, although very distorted. A high-enough applied electric field completely unwinds the macroscopic long-pitch helical structure and produces unwound Sm$C^*_A(1/3)$ with p_{qT} =3 and $q_E = 1/3$, which is similar to the three-layer superstructure stabilised in the condensation process of discrete solitons. Likewise, suppose that Sm$C^*_A(3/5)$ is to be stabilised from the high field side as pointed out above in connection with Figure 2(h), the characteristic relation similar to that between SmC^*_α and Sm$C^*_A(1/3)$ may be realised. Unwound Sm$C^*_A(3/5)$ with $p_{qT} = 5$ and $q_E = 1/5$ can be considered as the superstructure with a unit cell of five-layer periodicity stabilised by the condensation process. The temperature at which Sm$C^*_A(3/5)$ comes to exist at $E = 0$ in a particular material may correspond to the temperature where SmC^*_α has the short helical pitch of p_α=5 smectic layers. The detailed structural evolution at around 65 wt% will clarify whether Sm$C^*_A(3/5)$ is actually stabilised.

The situation must be slightly different in the case of SmC^*_α with $p_\alpha = 4$ and Sm$C^*_A(1/2)$; the superstructure with a unit cell of four-layer periodicity stabilised by the condensation process is different from Sm$C^*_A(1/2)$, which is antiferroelectric and may be destabilised by the applied field. However, it is tempting to consider that the temperature at which Sm$C^*_A(1/2)$ comes to exist at $E = 0$ in a particular material corresponds to the temperature where SmC^*_α has the short helical pitch of $p_\alpha = 4$ smectic layers. Whether this is the case or not can be checked experimentally by determining p_α directly as in (*39*) using mixtures with several MHPOOCBC concentrations between 38 and 50 wt%, as studied in Figure 2(d) and (e). Moreover, we can also anticipate the similar relation between Sm$C^*_A(1/4)$ and SmC^*_α with $p_\alpha = 8/3$. Note that antiferroelectric Sm$C^*_A(1/4)$ has $q_E = 0$ and $p_{qT} = 8/3$.

As stated in Section 3.1.1, it is well established that SmC^*_α directly adjoins $SmC^*_A(1/4)$ on the low-temperature side. In the case of the MHPOCBC–MHPOOCBC binary mixture system, $SmC^*_A(1/4)$ does not seem to exist in pure MHPOCBC but it does emerge at 38 wt% as shown in Figures 2(d) and 5. Therefore, $SmC^*_A(1/4)$ comes to exists at $E = 0$ in a particular concentration in between, and at the same time the shortest p_α of SmC^*_α may become 8/3. Experimentally, we need to determine p_α directly as is done in (*39*) and to obtain the *E–T* phase diagram by changing the concentration more minutely, so that we can see the detailed structural evolution. Theoretically, we have to study the boundary between biaxial phases and uniaxial SmC^*_α more accurately. These are interesting and important, theoretical and experimental studies to be performed in the near future.

Acknowledgements

We are pleased to contribute a paper, stimulated by de Gennes's basic idea of frustration, to this special issue of *Liquid Crystals*. We would like to acknowledge Mamoru Yamashita for enlightening discussions about the unwinding process of SmC^*_α as the condensation of discrete solitons. We are grateful to the Irish Research Council of Science, Engineering and Technology (IRCSET) for the award of a postdoctoral Fellowship to K. L. Sandhya for 2006–08. The experimental facilities were funded by the SFI (grant no. 02/IN.1/I031).

References

(1) Meyer, R. B.; Liebert, L.; Strzelecki, L.; Keller, P. *J. Phys. Lett. (France)* **1975**, *36*, L69–L71.
(2) Chandani, A. D. L.; Gorecka, E.; Ouchi, Y.; Takezoe, H.; Fukuda, A. *Jpn. J. Appl. Phys., Part 2* **1989**, *28*, L1265–L1268.
(3) de Gennes, P. G.; Prost, J. *The Physics of Liquid Crystals*, 2nd edn; Clarendon Press: Oxford, 1993, pp. 551–578.
(4) Prost, J.; Bruinsma, R. *Ferroelectrics* **1993**, *148*, 25–29.
(5) Bruinsma, R.; Prost, J. *J. Phys. (France)* **1994**, *4*, 1209–1219.
(6) Fukuda, A.; Takanishi, Y.; Isozaki, T.; Ishikawa, K.; Takezoe, H. *J. Mater. Chem*. **1994**, *4*, 997–1016.
(7) Mach, P.; Pindak, R.; Levelut, A.-M.; Barois, P.; Nguyen, H. T.; Huang, C. C.; Furenlid, L. *Phys. Rev. Lett*. **1998**, *81*, 1015–1018.
(8) Mach, P.; Pindak, R.; Levelut, A.-M.; Barois, P.; Nguyen, H. T.; Baltes, H.; Hird, M.; Toyne, K.; Seed, A.; Goodby, J. W.; Huang, C. C.; Furenlid, L. *Phys. Rev. E* **1999**, *60*, 6793–6802.
(9) Akizuki, T.; Miyachi, K.; Takanishi, Y.; Ishikawa, K.; Takezoe, H.; Fukuda, A. *Jpn. J. Appl. Phys., Part 1* **1999**, *38*, 4832–4837.
(10) Johnson, P. M.; Olson, D. A.; Pankratz, S.; Nguyen, T.; Goodby, J. W.; Hird, M.; Huang, C. C. *Phys. Rev. Lett*. **2000**, *84*, 4870–4873.
(11) Cady, A.; Pitney, J. A.; Pindak, R.; Matkin, L. S.; Watson, S. J.; Gleeson, H. F.; Cluzeau, P.; Barois, P.; Levelut, A.-M.; Caliebe, W.; Goodby, J. W.; Hird, M.; Huang, C. C. *Phys. Rev. E* **2001**, *64*, 050702-1-4.
(12) Matkin, L. S.; Watson, S. J.; Gleeson, H. F.; Pindak, R.; Pitney, J.; Johnson, P. M.; Huang, C. C.; Barois, P.; Levelut, A.-M.; Srajer, G.; Pollmann, J.; Goodby, J. W.; Hird, M. *Phys. Rev. E* **2001**, *64*, 021705-1-6.
(13) Cady, A.; Liu, Z. Q.; Han, X. F.; Wang, S. T.; Veum, M.; Janarthanan, N.; Hsu, C. S.; Olson, D. A.; Huang, C. C. *Phys. Rev. E* **2002**, *66*, 061704-1-6.
(14) Emelyanenko, A. V.; Osipov, M. A. *Phys. Rev. E* **2003**, *68*, 051703-1-16.
(15) Emelyanenko, A. V.; Osipov, M. A. *Ferroelectrics* **2004**, *309*, 13–25.
(16) Shtykov, N. M.; Chandani, A. D. L.; Emelyanenko, A. V.;, Fukuda, A.; Vij, J. K. *Phys. Rev. E* **2005**, *71*, 021711-1-12.
(17) Osipov, M. A.; Fukuda, A.; Hakoi, H.; *Mol. Cryst. Liq. Cryst*. **2003**, *402*, 9–30.
(18) Fukuda, A.; Hakoi, H.; Sato, M.; Osipov, M. A. *Mol. Cryst. Liq. Cryst*. **2003**, *398*, 169–187.
(19) Orihara, H.; Ishibashi, Y. *Jpn. J. Appl. Phys., Part 2* **1990**, *29*, L115–L118.
(20) Roy, A.; Madhusudana, N. V.; *Europhys. Lett.* **1996**, *36*, 221–226.
(21) Yamashita, M.; Takeno, S., *J. Phys. Soc. Jpn.* **1999**, *68*, 1473–1476.
(22) Matsumoto, T.; Fukuda, A.; Johno, M.; Motoyama, Y.; Yui, T.; Seomun, S.-S.; Yamashita, M. *J. Mater. Chem*. **1999**, *9*, 2051–2080.
(23) Cepic, M.; Zeks, B. *Phys. Rev. Lett*. **2001**, *87*, 085501-1-4.
(24) Cepic, M.; Gorecka, E.; Pociecha, D.; Zeks, B.; Nguyen, H. T. *J. Chem. Phys*. **2002**, *117*, 1817–1826.
(25) Olson, D. A.; Han, X. F.; Cady, A.; Huang, C. C. *Phys. Rev. E* **2002**, *66*, 021702-1-5.
(26) Dolganov, P. V.; Zhilin, V. M.; Dolganov, V. K.; Kats, E. I.; *Phys. Rev. E* **2003**, *67*, 041716-1-12.
(27) Hamanesh, B. N.; Taylor, P. L. *Phys. Rev. Lett*. **2004**, *93*, 167801-1-4.
(28) Isozaki, T.; Fujikawa, T.; Takezoe, H.; Fukuda, A.; Hagiwara, T.; Suzuki, Y.; Kawamura, I.; *Phys. Rev. B* **1993**, *48*, 13439–13450.
(29) Laux, V.; Isaert, N.; Nguyen, H. T.; Cluzeau, P.; Destrade, C.; *Ferroelectrics* **1996**, *179*, 25–31.
(30) Schlauf, D.; Bahr, C. *Phys. Rev. E* **1999**, *60*, 6816–6825.
(31) Johnson, P. M. Pankratz, S.; Mach, P.; Nguyen, H. T.; Huang, C. C.; *Phys. Rev. Lett*. **1999**, *83*, 4073–4076.
(32) Laux, V.; Isaert, N.; Joly, G.; Nguyen, H. T. *Liq. Cryst*. **1999**, *26*, 361–373.
(33) Laux, V.; Isaert, N.; Faye, V.; Nguyen, H. T.; *Liq. Cryst.* **2000**, *27*, 81–88.
(34) Olson, D. A.; Pankratz, S.; Johnson, P. M. Cady, A.; Nguyen, H. T.; Huang, C. C. *Phys. Rev. E* **2001**, *63*, 061711-1-8.
(35) Da Cruz, C.; Rouillon, J. C.; Marcerou, J. P.; Isaert, N.; Nguyen, H. T. *Liq. Cryst*. **2001**, *28*, 125–137.
(36) Shtykov, N. M.; Vij, J. K.; Nguyen, H. T. *Phys. Rev. E* **2001**, *63*, 051708-1-7.
(37) Cady, A.; Olson, D. A.; Han, X. F.; Nguyen, H. T.; Huang, C. C. *Phys. Rev. E* **2002**, *65*, 030701-1-4.
(38) Cady, A.; Han, X. F.; Olson, D. A.; Orihara, H.; Huang, C. C. *Phys. Rev. Lett.* **2003**, *91*, 125502-1-4.
(39) Liu, Z. Q.; McCoy, B. K.; Wang, S. T.; Pindak, R.; Caliebe, W.; Barois, P.; Fernandes, P.; Nguyen, H.

T.; Hsu, C. S.; Wang, S.; Huang, C. C. *Phys. Rev. Lett*. **2007**, *99*, 077802-1-4.
(40) Cepic, M.; Zeks, B. *Mol. Cryst. Liq. Cryst*. **1995**, *263*, 61–67.
(41) Torikai, M.; Yamashita, M. *Mol. Cryst. Liq. Cryst*. **2007**, *465*, 239–247.
(42) Sugimoto, Y.; Torikai, M.; Yamashita, M.; *Mol. Cryst. Liq. Cryst*. **2009**, *511*, 1818–1829.
(43) Sakai, Y.; Torikai, M.; Yamashita, M. *Mol. Cryst. Liq. Cryst.* **2009**, in press.
(44) Yokoi, C. S. O.; Tang, L.-H.; Chou, W. *Phys. Rev. B* **1988**, *37*, 2173–2198.
(45) Yamashita, M., in *Solitons in Liquid Crystals*, edited by Lam L. and Prost J. (Springer: Berlin, 1991), Chap. 10, pp. 293–325.
(46) de Gennes, P. G., in *Fluctuations, Instabilities, and Phase Transitions*; Nato Advanced Study Institute Series: Series B, Physics, 11, (Plenum Press: New York, 1975), Chap. 1, pp. 1–18.
(47) Takanishi, Y.; Hiraoka, K.; Agrawal, V. K.; Takezoe, H.; Fukuda, A.; Matsushita, M. *Jpn. J. Appl. Phys., Part 1* **1991**, *30*, 2023–2027.
(48) Hiraoka, K.; Takanishi, Y.; Skarp, K.; Takezoe, H.; Fukuda, A. *Jpn. J. Appl. Phys., Part 2* **1991**, *30*, L1819–L1822.
(49) Hiraoka, K.; Takanishi, Y.; Takezoe, H.; Fukuda, A. *Jpn. J. Appl. Phys., Part 1* **1992**, *31*, 3394–3398.
(50) Jaffe, B.; Cooke, W. R. Jr.; Jaffe, H.; *Piezoelectric Ceramics*; Academic Press: New York, 1971, p. 14.
(51) Takezoe, H.; Lee, J.; Ouchi, Y.; Fukuda, A. *Mol. Cryst. Liq. Cryst*. **1991**, *202*, 85–90.
(52) Miyachi, K.; Kabe, M.; Ishikawa, K.; Takezoe, H.; Fukuda, A. *Ferroelectrics* **1993**, *147*, 147–157.
(53) Sandhya, K. L.; Fukuda, A.; Vij, J. K. *Mol. Cryst. Liq. Cryst*. **2009**, *511*, 1506–1519.
(54) Panov, V. P.; Shtykov, N. M.; Fukuda, A.; Vij, J. K. Suzuki, Y.; Lewis, R. A.; Hird, M.; Goodby, J. W.; *Phys. Rev. E* **2004**, *69*, 060701-1-4.
(55) Chandani, A. D. L.; Shtykov, N. M.; Panov, V. P.; Emelyanenko, A. V.;, Fukuda, A.; Vij, J. K. *Phys. Rev. E* **2005**, *72*, 041705-1-13.
(56) Orihara, H.; Naruse, Y.; Yagyu, M.; Fajar, A.; Uto, S. *Phys. Rev. E* **2005**, *72*, 040701-1-4.
(57) Billardon, M.; Badoz, J. *C. R. Acad. Sci. Paris* **1966**, *262*, 1672–1675.
(58) Jasperson, S. N.; Schnatterly, S. E. *Rev. Sci. Instrum*. **1969**, *40*, 761–766.
(59) Mollenauer, L. F.; Downie, D.; Engstrom, H.; Grant, W. B. *Appl. Opt.* **1969**, *8*, 661–665.
(60) Kemp, J. C. *J. Opt. Soc. Am* **1969**, *59*, 950–954.
(61) Breeze, R. H.; Ke, B. *Anal. Biochem*. **1972**, *50*, 281–303.
(62) Kondo, K.; Muta, K.; Akiyama, R.; Fukuda, A.; Kuze, E. *Sen-i Gakkaishi* **1980**, *36*, T465–T471.
(63) Emelyanenko, A. V.; Fukuda, A.; Vij, J. K. *Phys. Rev. E* **2006**, *74*, 011705-1-17.
(64) (a) Li, J.; Takezoe, H.; Fukuda, A. *Jpn. J. Appl. Phys*. **1991**, *30*, 532–536. (b) Lagerwell, J. P. F.; Giesselmann, F.; Osipov, M. *Liq. Cryst*. **2006**, *33*, 625.
(65) Okabe, N.; Suzuki, Y.; Kawamura, I.; Isozaki, T.; Takezoe, H.; Fukuda, A. *Jpn. J. Appl. Phys., Part 2* **1992**, *31*, L793–L796.
(66) Yamashita, M.; Miyazima, S. *Ferroelectrics* **1993**, *148*, 1–9.
(67) Osipov, M. A.; Gorkunov, M. V. *Liq. Cryst*. **2006**, *33*, 1133–1141.
(68) Song, J. K.; Fukuda, A.; Vij, J. K. *Phys. Rev. E* **2008**, *78*, 041702-1-12.
(69) Pociecha, D.; Gorecka, E.; Cepic, M.;, Vaupotic, N.; Zeks, V.; Kardas, D.; Mieczkowski, J. *Phys. Rev. Lett*. **2001**, *86*, 3048–3051.
(70) Wang, S. T.; Liu, Z. Q.; McCoy, B. K.; Pindak, R.; Caliebe, W.; Nguyen, H. T.; Huang, C. C. *Phys. Rev. Lett*. **2007**, *96*, 097801-1-4.
(71) Sandhya, K. L.; Panarin, Yu. P.; Manna, U.; Vij, J. K.; Kumar, S. *Phys. Rev. Lett*. **2007**, *98*, 219801.
(72) Hiraoka, K.; Takezoe, H.; Fukuda, A. *Ferroelectrics* **1993**, *147*, 13–25.
(73) Panarin, Yu. P.; Kalinovskaya, O.; Vij, J. K. *Liq. Cryst*. **1998**, *25*, 241–252.
(74) Buivydas, M.; Gouda, F.; Lagerwall, S.; Stebler, B. *Liq. Cryst*. **1995**, *18*, 879–886.
(75) Buivydas, M.; Gouda, F.; Andersson, G.; Lagerwall, S.; Stebler, B.; Bomelburg, J.; Heppke, G.; Gestblom, B. *Liq. Cryst*. **1997**, *23*, 723–739.
(76) Parry-Jones, L. A. Elston, S. J. *Phys. Rev. E* **2001**, *63*, 050701-1-4.
(77) Shtykov, N. M.; Vij, J. K. Lewis, R. A.; Hird, M.; Goodby, J. W. *Phys. Rev. E* **2000**, *62*, 2279–2287.
(78) Manjuladevi, V.; Vij, J. K. *Liq. Cryst*. **2007**, *34*, 963–973.
(79) Jaradat, S.; Brimicombe, P. D.; Southern, C.; Siemianowski, S. D.; DiMasi, E.; Osipov, M.; Pindak, R.; Gleeson, H. F. *Phys. Rev. E* **2008**, *77*, 010701-1-4.
(80) Marcerou, J. P.; Nguyen, H. T.; Bitri, N.; Gharbi, A.; Essid, S.; Soltani, T. *Europhys. J. E* **2007**, *23*, 319–328.
(81) Hiraoka, K.; Chandani, A. D. L.; Gorecka, E.; Ouchi, Y.; Takezoe, H.; Fukuda, A. *Jpn. J. Appl. Phys., Part 2* **1990**, *29*, L1473–L1476.
(82) Song, J.-K.; Chandani, A. D. L.; Fukuda, A.; Vij, J. K.; Kobayashi, I.; Emelyanenko, A. V. *Phys. Rev. E* **2007**, *76*, 011709-1-13.
(83) Song, J.-K.; Fukuda, A.; Vij, J. K. *Phys. Rev. Lett*. **2008**, *101*, 097801-1-4.

Appendix 1. Polarisation-dependent free energy in Sm-C^*_α

According to (*14*, *16*), the polarisation-dependent terms in the free energy per a smectic layer can be rewritten as

$$\Delta F_i = \frac{1}{2\chi}\{\mathbf{P}_i^2 + g(\mathbf{P}_i \cdot \mathbf{P}_{i+1} + \mathbf{P}_i \cdot \mathbf{P}_{i-1})\} + \mathbf{P}_i \cdot \mathbf{M}_i, \qquad (A.1)$$

where

$$\mathbf{M}_i \equiv c_\mathrm{p} \cos\theta\,[\mathbf{n}_i \times \mathbf{k}] + c_\mathrm{f} \cos\theta\,\Delta\mathbf{n}_{i\pm1}. \qquad (A.2)$$

By minimising the whole free energy (which is a sum of Equation (A.1) over all smectic layers) with respect to all polarisation vectors, we obtain

$$\mathbf{P}_i + g(\mathbf{P}_{i-1} + \mathbf{P}_{i+1}) = -\chi\mathbf{M}_i. \qquad (A.3)$$

By substituting Equation (A.3) back into Equation (A.1), we obtain

$$\Delta F_i = \frac{1}{2}\mathbf{P}_i \cdot \mathbf{M}_i, \qquad (A.4)$$

where the parameters $\mathbf{M}_i$ are given by Equation (A.2). A set of Equations (A.3) can be solved for any biaxial subphase with a particular unit cell (*14*).

Since the microscopic short-pitch helical structure is numerically proved to emerge around the frustration point P_α as already shown in Figure 9 of (*16*), we can easily obtain the following expression in SmC^*_α:

$$\mathbf{P}_i = -\frac{\chi}{1 + 2g\cos\Delta\varphi}\mathbf{M}_i, \tag{A.5}$$

where $\Delta\varphi = \varphi_{i+1} - \varphi_i$ is the **c**-director twist angle between adjacent layers. Substituting Equation (A.5) into Equation (A.1) and introducing the coordinates for vector $\mathbf{n}_i$ according to

$$\mathbf{n}_i = \sin\theta(\mathbf{x}\cos\varphi_i + \mathbf{y}\sin\varphi_i) + \mathbf{k}\cos\theta, \tag{A.6}$$

where **x** and **y** are some orthogonal unit vectors in the layer plane, the polarisation-dependent part of the free energy in SmC^*_α per one smectic layer is given as

$$\Delta F_i = -\frac{\chi}{2(1 + 2g\cos\Delta\varphi)}\sin^2\theta \times (c_\mathrm{p}^2 + c_\mathrm{f}^2\sin^2\Delta\phi - 2c_\mathrm{p}c_\mathrm{f}\sin\Delta\phi). \tag{A.7}$$

Thus, by using the analytical expression (A.7) together with the free energy F_i that does not depend on the polarisation given in Equation (18) of (*16*), we can easily explain the characteristic features of SmC^*_α pointed out in Section 3.3.1 and at the same time always have the continuous change from SmC^*_α to not only SmC^*_A but also Sm*C**. Even when we use a much more simplified phenomenological F_i given by Equation (1) of (*83*), we arrive at the same conclusion.